Writing Method of Moments code for Inverse Source Reconstruction Algorithm

Aryan Gupta

220108011

EE 498 B.Tech. Project - III

Project Report

Supervisor

Prof. Ashwini Sawant

November 7, 2025

DEPARTMENT OF ELECTRONICS AND ELECTRICAL ENGINEERING

INDIAN INSTITUTE OF TECHNOLOGY, GUWAHATI

GUWAHATI, 781039

Abstract

This project presents the development of an in-house electromagnetic solver for antenna near-field to far-field transformation using an inverse source method. The work is based on a problem statement released by ISRO, which aims to replace commercial electromagnetic solvers with an indigenous, fully open-source implementation.

The developed code numerically reconstructs the equivalent surface currents on a Huygens' surface from given near-field electric field data. These currents are then used to estimate the far-field radiation pattern of directive antennas. The present implementation assumes an ideal scenario—the input electric field excitation is noise-free and perfectly known. Under these conditions, the code produces theoretically correct and consistent results, validating the mathematical model and numerical formulation.

Although the current version is not yet suited for real measurement data, it establishes the computational foundation for future extensions. In the next phase, the solver will be enhanced to handle noisy and incomplete near-field data, enabling its application in practical antenna characterization and measurement systems at ISRO facilities.

CONTENTS

I. Introduction

Large parabolic reflector antennas used by ISRO play a critical role in satellite communication, deep-space telemetry, and tracking operations. The performance of these antennas depends heavily on the precise alignment and integrity of every individual panel on the reflector surface. Even small structural deviations, surface defects, or alignment errors on a single panel can significantly distort the radiation pattern, reduce gain, or introduce unexpected sidelobes. Diagnosing such issues is currently a labor-intensive process, often requiring manual inspection of each panel, which is time-consuming, costly, and difficult for large apertures installed at operational sites.

To address this challenge, ISRO is exploring the use of drones attached with antennas to measure the near-field electric field around the antenna while it is operating. By processing this measured field, it is possible to recover the surface current distribution on the reflector and reconstruct the far-field radiation pattern, enabling engineers to identify which specific region of the parabolic surface is degrading performance. This approach provides a non-contact, automated method of diagnosing reflector health, eliminating the need for commercial electromagnetic simulation tools and allowing fully in-house processing tailored to ISRO's requirements.

This project focuses on developing a Python-based Method of Moments (MoM) solver capable of computing surface currents, near-field and far-field quantities directly from measured data, and evaluating the condition of individual reflector panels. The aim is to create a reliable, open source, and customizable electromagnetic analysis pipeline that can be integrated into ISRO's drone-based antenna inspection workflow.

II. Methodology

In this section, the key methodological choices made during the project are discussed, including the rationale for selecting the Method of Moments (MoM) over the Finite Element Method (FEM), and the decision to employ Rao–Wilton–Glisson (RWG) basis functions instead of alternative formulations. This section also describes the process of design and meshing, which was carried without using licensed software tools such as Autodesk Fusion 360 for geometric modeling and MATLAB by MathWorks for computational processing and simulation.

A. Method of Moments

In the Method of Moments, the unknown surface current density is represented as a weighted sum of predefined basis functions, allowing the continuous problem to be converted into a finite-

dimensional system. Specifically, the current J(r) is expanded as a linear combination of N basis functions, and the integral equation involving the operator is rewritten as an integral involving the Green's function, which acts as the inverse of that operator. By substituting the basis expansion into this integral equation and applying a testing function, we obtain one algebraic equation for each basis coefficient. Using the same number of testing functions as basis functions produces a closed system of N equations. When the testing functions are chosen to be identical to the basis functions, the procedure is known as Galerkin's method. In this work, the Rao–Wilton–Glisson (RWG) basis functions are employed, as they are widely used for representing currents on triangulated surfaces due to their continuity and physical correctness.

Unlike the Method of Moments, which naturally handles open-region surface problems, the Finite Element Method (FEM) is primarily suited for volume-based electromagnetic problems. FEM requires discretizing the entire three-dimensional region around the structure, including air or vacuum, which significantly increases the number of unknowns. It is most effective when dealing with inhomogeneous materials, waveguides, cavities, or geometries where the fields are confined to a finite volume. On the other hand, the Finite Difference Time Domain (FDTD) method operates in the time domain, making it well-suited for transient analysis, broadband simulations, and pulse propagation problems. FDTD also requires discretizing the entire computational space and relies on absorbing boundary conditions such as PML to simulate open regions. Because our problem involves time-harmonic fields radiating from a PEC surface and does not require volumetric meshing, MoM provides a more efficient and accurate formulation compared to FEM and FDTD [1].

$$\mathbf{J}(\mathbf{r}) \approx \sum_{n=1}^{N} I_n \, \mathbf{b}_n(\mathbf{r}), \tag{1}$$

$$\mathcal{L}\{\mathbf{J}(\mathbf{r})\} = \mathbf{E}^{\text{inc}}(\mathbf{r}), \tag{2}$$

$$\mathcal{L}\{G(\mathbf{r}, \mathbf{r}')\} = \delta(\mathbf{r} - \mathbf{r}'), \tag{3}$$

$$\mathcal{L}^{-1}\{f(\mathbf{r})\} = \int G(\mathbf{r}, \mathbf{r}') f(\mathbf{r}') \, dS'. \tag{4}$$

$$\mathbf{E}^{\text{inc}}(\mathbf{r}) = \int G(\mathbf{r}, \mathbf{r}') \, \mathbf{J}(\mathbf{r}') \, dS'. \tag{5}$$

$$\mathbf{E}^{\text{inc}}(\mathbf{r}) = \sum_{n=1}^{N} I_n \int G(\mathbf{r}, \mathbf{r}') \, \mathbf{b}_n(\mathbf{r}') \, dS'. \tag{6}$$

$$\left\langle \mathbf{b}_m,\, \mathbf{E}^{\text{inc}} \right\rangle = \sum_{n=1}^{N} I_n \left\langle \mathbf{b}_m(\mathbf{r}),\, \int G(\mathbf{r},\mathbf{r}')\mathbf{b}_n(\mathbf{r}')\, dS' \right\rangle. \tag{7}$$

$$Z_{mn} = \left\langle \mathbf{b}_m(\mathbf{r}),\, \int G(\mathbf{r},\mathbf{r}')\mathbf{b}_n(\mathbf{r}')\, dS' \right\rangle, \tag{8}$$

$$V_m = \left\langle \mathbf{b}_m, \mathbf{E}^{\text{inc}} \right\rangle. \tag{9}$$

$$\mathbf{Z}\,\mathbf{I} = \mathbf{V}. \tag{10}$$

B. Numerical Integration

Gaussian quadrature is a numerical integration technique that approximates surface integrals by evaluating the integrand at specific weighted points within the domain. When applied to triangular surfaces, the integral is transformed into a weighted sum of function values evaluated at predetermined barycentric coordinates inside the triangle. This approach provides high accuracy with relatively few evaluation points, making it well-suited for Method of Moments formulations where double surface integrations are required. For this project I tested with 3, 4, 6, 7, 12 and 16-point Gaussian Quadrature but there are higher order ones as well [2].

$$\vec{r} = \gamma\vec{v}_1 + \alpha\vec{v}_2 + \beta\vec{v}_3$$

$$\iint_T f(\vec{r})\, dS \approx A \sum_{i=1}^{M} w(\alpha_i, \beta_i, \gamma_i)\, f(\alpha_i, \beta_i, \gamma_i)$$

C. Basis Functions

The Rao-Wilton-Glisson (RWG) basis function is widely used in the Method of Moments (MoM) to model surface current distributions on triangulated conducting surfaces. It defines a piecewise-linear current flowing between two adjacent triangular elements that share a common edge. The RWG function ensures continuity of the normal current component across this shared edge while vanishing on the outer edges, accurately representing surface current behavior. Its simplicity, locality, and compatibility with triangular meshes make it a standard choice for electromagnetic surface integral equation formulations [3].

$$\mathbf{f}_n(\mathbf{r}') = \begin{cases} \dfrac{l_n}{2A_n^+}\, \boldsymbol{\rho}_n^+(\mathbf{r}'), & \mathbf{r}' \in T_n^+, \\ -\dfrac{l_n}{2A_n^-}\, \boldsymbol{\rho}_n^-(\mathbf{r}'), & \mathbf{r}' \in T_n^-, \\ 0, & \text{elsewhere.} \end{cases} \tag{11}$$

TABLE I: Six- and Seven-Point Quadrature Rules

Table 9.3: Six-Point Quadrature Rule

i	α	β	γ	w
1	0.10810301	0.44594849	0.44594849	0.22338158
2	0.44594849	0.10810301	0.44594849	0.22338158
3	0.44594849	0.44594849	0.10810301	0.22338158
4	0.81684757	0.09157621	0.09157621	0.10995174
5	0.09157621	0.81684757	0.09157621	0.10995174
6	0.09157621	0.09157621	0.81684757	0.10995174

Table 9.4: Seven-Point Quadrature Rule

i	α	β	γ	w
1	0.33333333	0.33333333	0.33333333	0.22500000
2	0.05971587	0.47014206	0.47014206	0.13239415
3	0.47014206	0.05971587	0.47014206	0.13239415
4	0.47014206	0.47014206	0.05971587	0.13239415
5	0.79742698	0.10128650	0.10128650	0.12593918
6	0.10128650	0.79742698	0.10128650	0.12593918
7	0.10128650	0.10128650	0.79742698	0.12593918

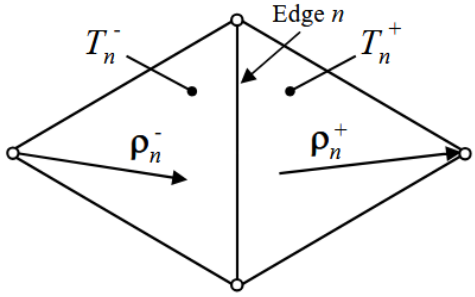

Fig. 1: RWG Basis Function

D. Designing

For designing the antennas I went with FreeCAD since its an open source software with nearly the same capabilities as Autodesk's Fusion 360 which is usually the go-to for doing any CAD modelling. We first do our modeling then export the model in .step format which can then be used by Gmsh for meshing the model.

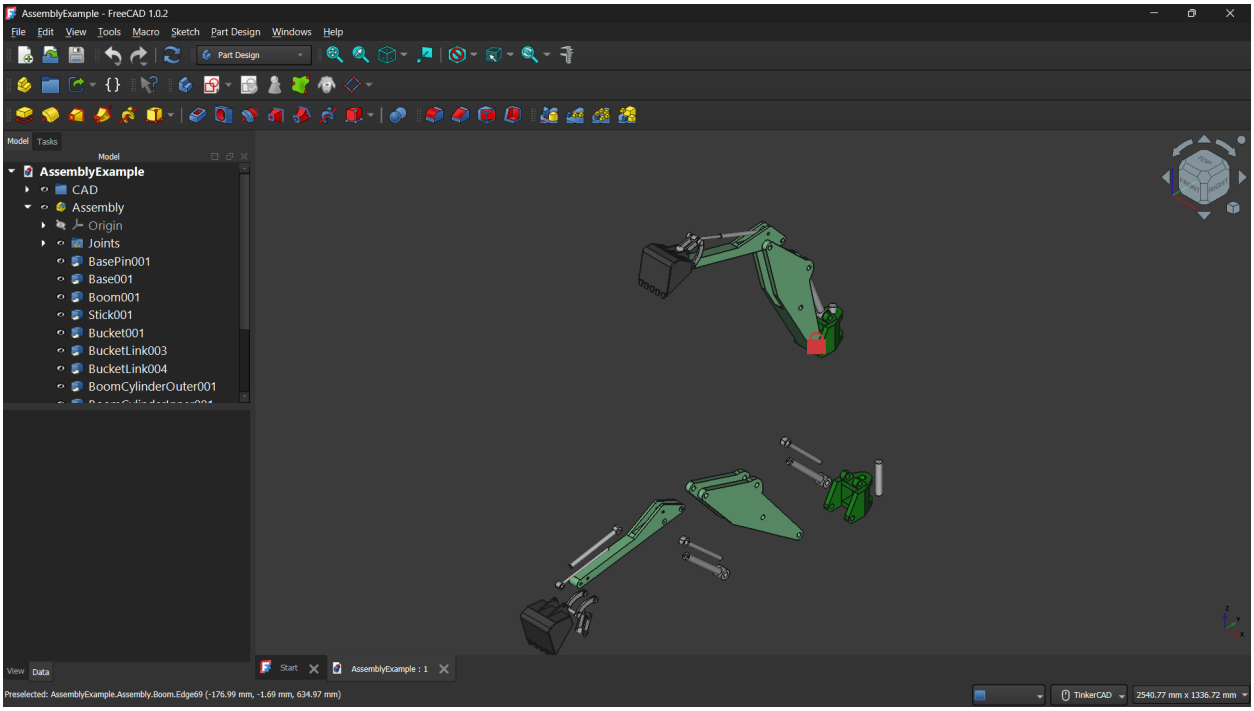

Fig. 2: Modelling in FreeCAD

E. Meshing

Gmsh is an open-source tool used to divide complex 3D geometries into smaller elements called meshes. In this project, it was used to create triangular surface meshes for the antenna models. Gmsh allows easy control over the mesh size and refinement It can also export mesh data in formats that work well with MATLAB and Python, making it convenient for custom electromagnetic solvers. Gmsh also has a Python module which allows us to easily integrate it with our code for purposes like increasing mesh size and checking convergence directly in our code.

F. Electric Field Integral Equations (EFIE)

These equations are derived and discussed in the book by Walton C. Gibson called The Method of Moments in Electromagnetics [3] and I followed the seminar conducted by Professor Jordan Budhu for getting a better understand on how to integrate everything together [4].

$$Z = \frac{L_m L_n}{A_m A_n} \iint_{T_m} \iint_{T_n} \left[\frac{1}{4} \vec{\rho}_m^{\pm}(\vec{r}) \cdot \vec{\rho}_n^{\pm}(\vec{r}\,') \pm \frac{1}{k^2} \right] \frac{e^{-jkr}}{4\pi r} \, d\vec{r}\,' \, d\vec{r} \tag{12}$$

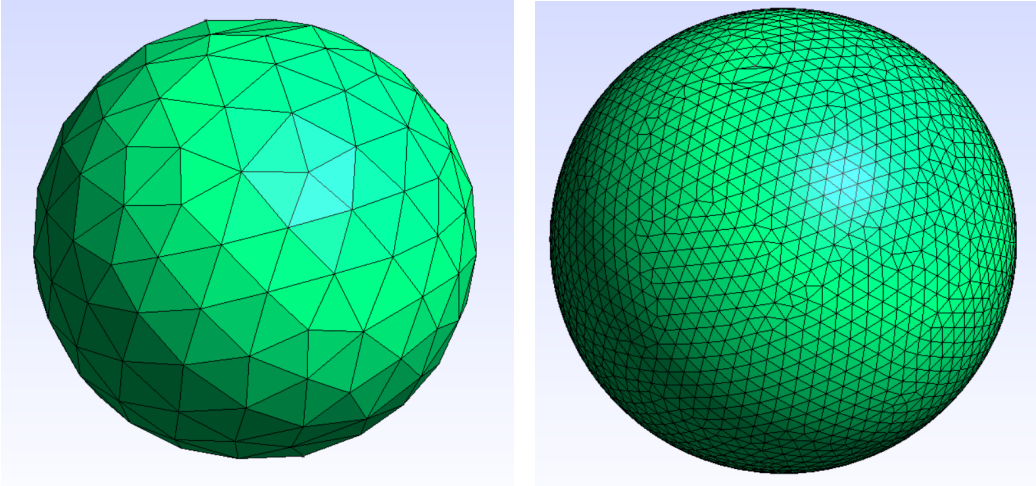

Fig. 3: Increasing mesh size

$$Z \approx \frac{L_m L_n}{4\pi} \sum_{p=1}^{M} \sum_{q=1}^{M} w_p w_q \left[\frac{1}{4} \vec{\rho}_m^{\pm}(\vec{r}_p) \cdot \vec{\rho}_n^{\pm}(\vec{r}_q^{'}) \pm \frac{1}{k^2} \right] \frac{e^{-jkR_{pq}}}{R_{pq}} \tag{13}$$

The equations below help up deal with the singularities that occur when the triangles of two different RWG basis functions are overlapping or side by side each other.

$$\vec{\rho}^{\pm} = \vec{r}^{\pm} - \hat{n}(\hat{n} \cdot \vec{r}^{\pm}) \tag{14}$$

$$\hat{l} = \frac{\vec{\rho}^{+} - \vec{\rho}^{-}}{|\vec{\rho}^{+} - \vec{\rho}^{-}|} \tag{15}$$

$$\hat{u} = \hat{l} \times \hat{n} \tag{16}$$

$$l^{\pm} = (\vec{\rho}^{\pm} - \vec{\rho}) \cdot \hat{l} \tag{17}$$

$$P^0 = |(\vec{\rho}^{\pm} - \vec{\rho}) \cdot \hat{u}| \tag{18}$$

$$P^{\pm} = |\vec{\rho}^{\pm} - \vec{\rho}| = \sqrt{(P^0)^2 + (l^{\pm})^2} \tag{19}$$

$$\hat{P}^0 = \frac{(\vec{\rho}^{\pm} - \vec{\rho}) - l^{\pm}\hat{l}}{P^0} \tag{20}$$

$$R^0 = \sqrt{(P^0)^2 + d^2} \tag{21}$$

$$R^{\pm} = \sqrt{(P^{\pm})^2 + d^2} \tag{22}$$

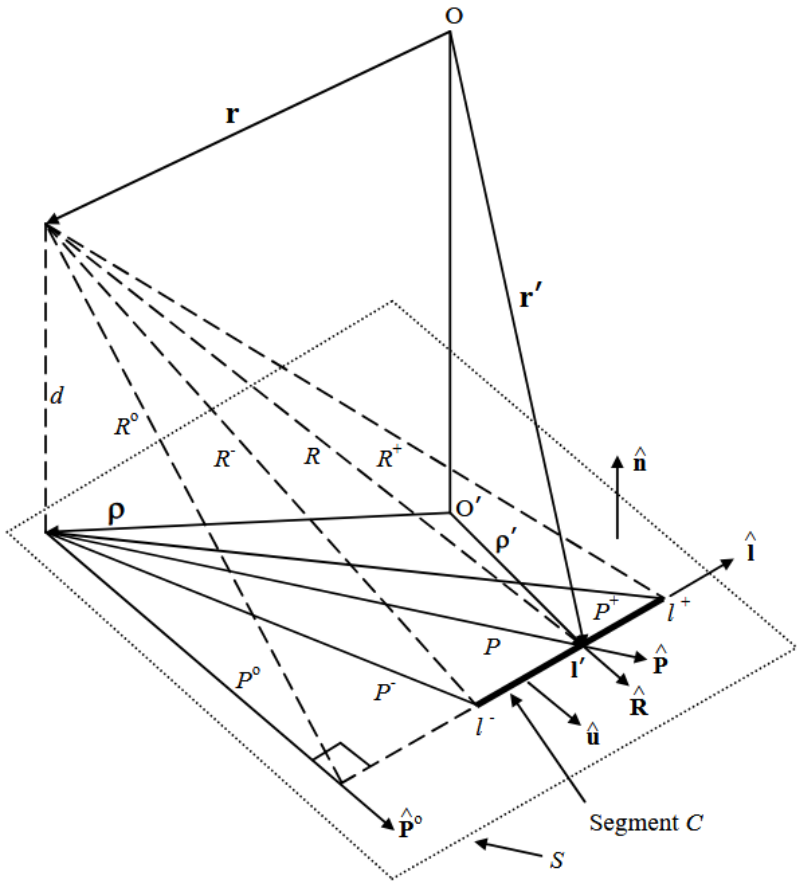

Fig. 4: Quantities used for dealing with singularies

$$d = \hat{n} \cdot (\vec{r} - \vec{r}^{\pm}) \tag{23}$$

$$I_1 = \iint_{T'} \frac{\vec{\rho}' - \vec{\rho}}{r} \, d\vec{r}' \tag{24}$$

$$I_1 = \frac{1}{2} \sum_{i=1}^{N} \hat{u}_i \left[(R_i^0)^2 \ln\left(\frac{R_i^+ + l_i^+}{R_i^- + l_i^-} \right) + l_i^+ R_i^+ - l_i^- R_i^- \right] \tag{25}$$

$$I_2 = \iint_{T'} \frac{1}{r} \, d\vec{r}' \tag{26}$$

$$\tag{27}$$

$$I_2 = \sum_{i=1}^{N} \hat{P}_i^0 \cdot \hat{u}_i \left[P_i^0 \ln\left(\frac{R_i^+ + l_i^+}{R_i^- + l_i^-} \right) - |d| \left(\tan^{-1}\left(\frac{P_i^0 l_i^+}{(R_i^0)^2 + |d| R_i^+} \right) - \tan^{-1}\left(\frac{P_i^0 l_i^-}{(R_i^0)^2 + |d| R_i^-} \right) \right) \right]$$

$$\rho_n(\vec{r}') = \vec{\rho}' - \vec{\rho}_n \tag{28}$$

$$\vec{\rho}' - \vec{\rho}_n = (\vec{\rho}' - \vec{\rho}) + (\vec{\rho} - \vec{\rho}_n) \tag{29}$$

$$\iint_{T'} \frac{\vec{\rho}_n(\vec{r}\,')}{r}\, d\vec{r}\,' = \iint_{T'} \frac{\vec{\rho}\,' - \vec{\rho}}{r}\, d\vec{r}\,' + (\vec{\rho} - \vec{\rho}_n) \iint_{T'} \frac{1}{r}\, d\vec{r}\,' \tag{30}$$

$$I_{mn}^{\pm\pm} = \frac{L_m L_n}{4\pi A_m A_n} \iint_{T_m^{\pm}} \iint_{T_n^{\pm}} \left[\frac{j\omega\mu}{4} \vec{\rho}_m^{\pm}(\vec{r}) \cdot \vec{\rho}_n^{\pm}(\vec{r}\,') \pm \frac{j}{\omega\varepsilon} \right] \left[\left(\frac{e^{-jkR}}{R} - \frac{1}{R} \right) + \frac{1}{R} \right] d\vec{r}\,'\, d\vec{r}$$

$$= \frac{L_m L_n}{4\pi A_m A_n} \iint_{T_m^{\pm}} \iint_{T_n^{\pm}} \left[\frac{j\omega\mu}{4} \vec{\rho}_m^{\pm}(\vec{r}) \cdot \vec{\rho}_n^{\pm}(\vec{r}\,') \pm \frac{j}{\omega\varepsilon} \right] \left(\frac{e^{-jkR}}{R} - \frac{1}{R} \right) d\vec{r}\,'\, d\vec{r} +$$

$$\frac{L_m L_n}{4\pi A_m A_n} \iint_{T_m^{\pm}} \iint_{T_n^{\pm}} \left[\frac{j\omega\mu}{4} \vec{\rho}_m^{\pm}(\vec{r}) \cdot \vec{\rho}_n^{\pm}(\vec{r}\,') \right] \frac{1}{R} d\vec{r}\,'\, d\vec{r} + \frac{L_m L_n}{4\pi A_m A_n} \iint_{T_m^{\pm}} \iint_{T_n^{\pm}} \left(\pm \frac{j}{\omega\varepsilon} \right) \frac{1}{R} d\vec{r}\,'\, d\vec{r}$$

The equation below shows how we integrate the electric field with the testing function, which in this case is same as the basis functions due to the use of Galerkin's method. The electric field we are using for testing is a plane wave travelling is z-direction polarized along the x-axis. This gives us the column vector which we mutliply with the inverse of impedence matrix to get the coefficients for each basis function.

$$I_m = \frac{L_m}{2A_m} \iint_{T_m^{\pm}} \vec{\rho}_m^{\pm}(\vec{r}) \cdot \vec{E}^i(\vec{r})\, d\vec{r} \approx \frac{L_m}{2} \sum_{p=1}^{M} w_p\, \vec{\rho}_m^{\pm}(\vec{r}_p^{\,\prime}) \cdot \vec{E}^i(\vec{r}_p^{\,\prime}) \tag{31}$$

Once we get all the coefficients for the basis functions we can use those to find the far field radiation pattern for the structure using the formulas given below. We again use Gaussian Quadrature to evaluate the integral efficiently.

$$\vec{E}_m(\vec{r}) = -\frac{j\omega\mu e^{-jkr}}{4\pi r} \frac{a_m L_m}{2A_m} \iint_{T_m} \vec{\rho}_m^{\pm}(\vec{r}\,') e^{jk\vec{r}\,'\cdot\hat{r}}\, d\vec{r}\,' \tag{32}$$

$$\vec{E}_m(\vec{r}) = -\frac{j\omega\mu e^{-jkr}}{4\pi r} \frac{a_m L_m}{2} \sum_{p=1}^{M} w_p\, \vec{\rho}_m^{\pm}(\vec{r}_p^{\,\prime}) e^{jk\vec{r}_p^{\,\prime}\cdot\hat{r}} \tag{33}$$

III. Results

The testing below was done for a plane structure divided into 3548 triangles and containing 5244 RWG Basis Functions.

TABLE II: Runtime comparison for different Gaussian Quadrature rules over triangular domains

Quadrature Rule	Runtime
3-point	1:39:18
4-point	1:43:32
6-point	1:47:14
7-point	1:52:05
12-point	2:17:38
16-point	2:41:26

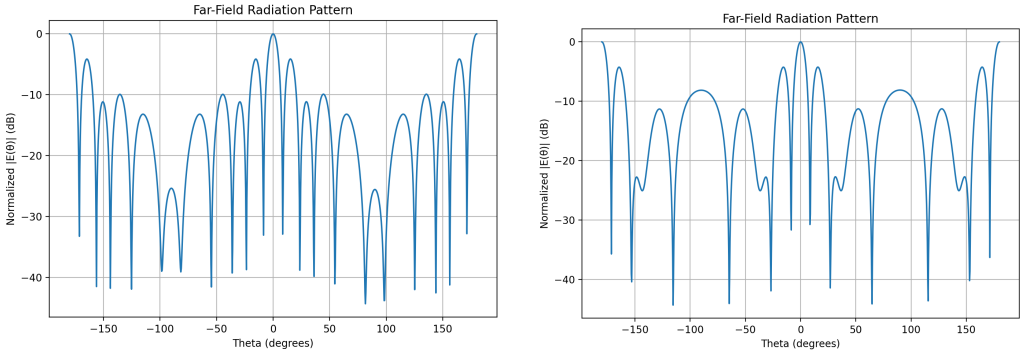

Fig. 5: 3 point vs 7 point Gaussian Quadrature

IV. Future Works

Future work includes improving the treatment of singular integrals for increased numerical accuracy, designing and simulating a parabolic antenna model to validate the implementation, and exploring Cython to accelerate the computationally intensive parts of the code. Additional goals involve learning to use PreProMAX for assigning realistic material properties to antenna surfaces, incorporating antenna weighting functions to account for practical measurement scenarios—such as electric field data collected by drones, where the onboard sensor does not record the true field directly—and implementing algorithms that reconstruct the far-field radiation pattern from near-field measurements.

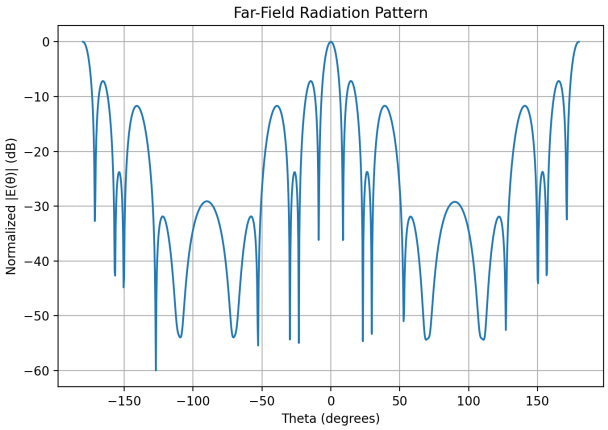

Fig. 6: Using 16-point Gauss Quadrature

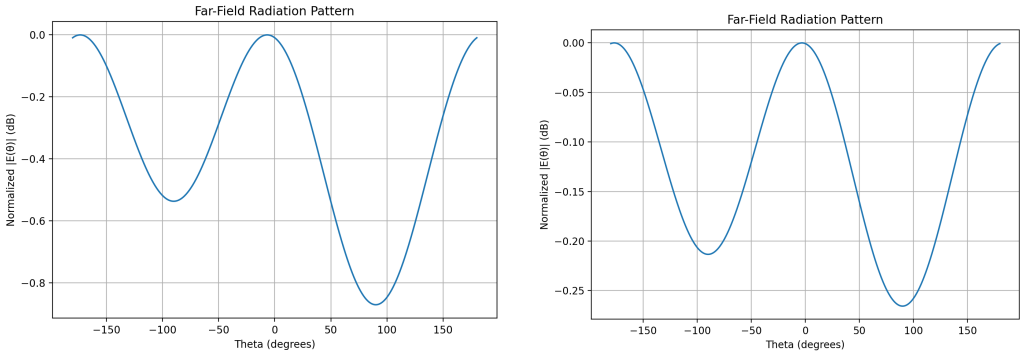

Fig. 7: Coarse (1986 triangles) vs very fine meshing (5626 triangles)

V. Conclusion

The current implementation requires further refinement in the treatment of singular integrals; however, the solver is now producing symmetric and consistent results. For planar geometries, the far-field radiation pattern shows peak responses that are closer together than expected. This behaviour is most likely due to the simplified singularity-handling scheme currently employed.

The numerical experiments also demonstrate that both excessively fine and overly coarse mesh discretisations lead to degraded accuracy, which aligns with theoretical expectations. An optimal mesh density therefore exists, beyond which improvements either stagnate or deteriorate.

The runtime analysis indicates that the 12-point Gaussian quadrature rule increases computation time by approximately 30% compared to the 7-point rule, while providing improved accuracy in the evaluated integrals. Since all simulations were executed on a laptop, the relative

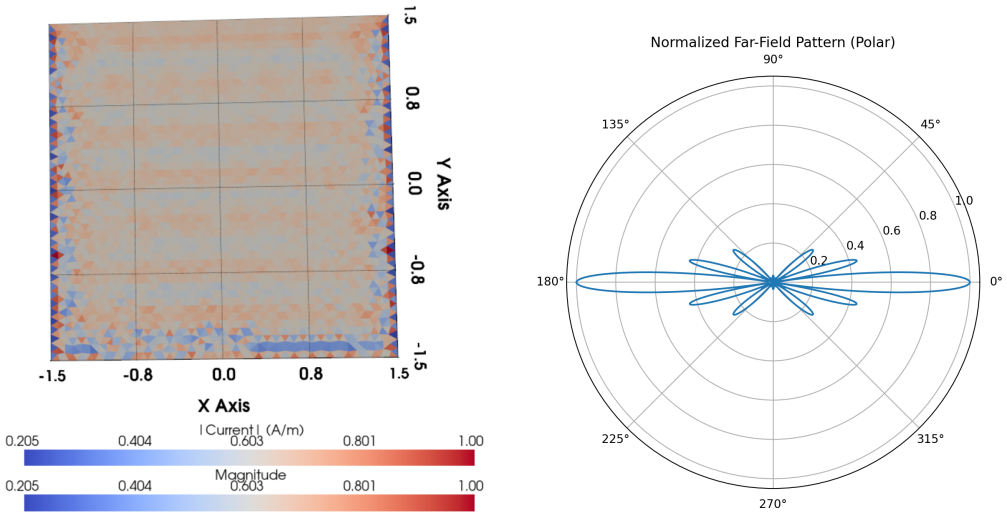

Fig. 8: Current distribution of planar structure (3571 triangles) and its polar plot

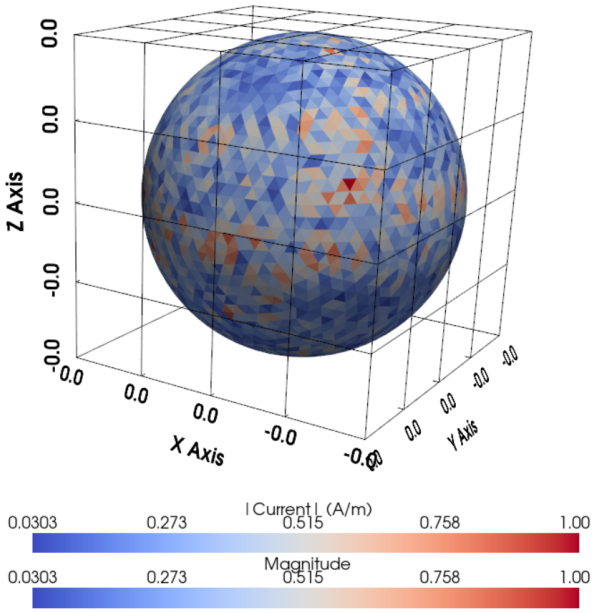

Fig. 9: Current Distribution for a sphere

performance gap is expected to be smaller on workstation-class hardware.

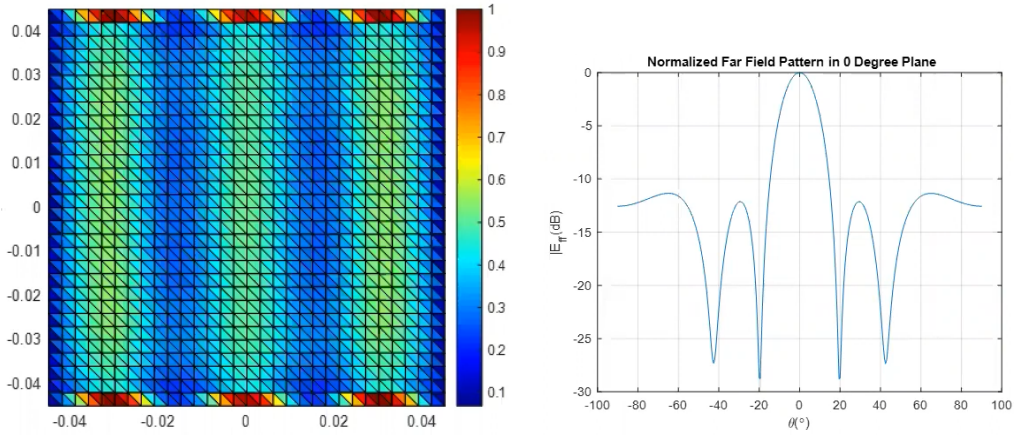

Fig. 10: Actual result for planar structure

REFERENCES

[1] C. S. Analysis, "Fdtd vs. fem vs. mom: What are they and how are they different?." https://resources.system-analysis.cadence.com/blog/msa2021-fdtd-vs-fem-vs-mom-what-are-they-and-how-are-they-different, 2021. Accessed: 2025-11-09.

[2] D. A. DUNAVANT, "High degree efficient symmetrical gaussian quadrature rules for the triangle." https://www2.karlin.mff.cuni.cz/~knobloch/FILES/MKP_20_21/g_quadr.pdf?utm_source=chatgpt.com, 1985. Accessed: 2025-11-09.

[3] W. C. Gibson, *The Method of Moments in Electromagnetics*. Chapman and Hall/CRC, 1 ed., 2008.

[4] L. B. D. J. Budhu, "Seminar on 3d method of moments for arbitrary shaped metasurfaces using rwg basis by dr jordan budhu." https://www.youtube.com/watch?v=4wODcAIIWxg, Nov 11, 2020. Accessed: 2025-09-26.